

# Stop as a next-to-lightest supersymmetric particle in constrained MSSM

Katri Huitu\* and Lasse Leinonen†

*Department of Physics, and Helsinki Institute of Physics, FIN-00014 University of Helsinki, Finland*

Jari Laamanen‡

*Theoretical High Energy Physics, IMAPP, Faculty of Science, Radboud University Nijmegen,  
Mailbox 79, P.O. Box 9010, NL-6500 GL Nijmegen, The Netherlands*

So far the squarks have not been detected at the LHC indicating that they are heavier than a few hundred GeVs, if they exist. The lighter stop can be considerably lighter than the other squarks. We study the possibility that a supersymmetric partner of the top quark, stop, is the next-to-lightest supersymmetric particle in the constrained supersymmetric standard model. Various constraints, on top of the mass limits, are taken into an account, and the allowed parameter space for this scenario is determined. Observing stop which is the next-to-lightest supersymmetric particle at the LHC may be difficult.

PACS numbers: 11.30.Pb, 12.60.Jv, 14.80.Ly, 13.85.-t  
Keywords: Stop NLSP, CMSSM

## I. INTRODUCTION

The next-to-lightest supersymmetric particle (NLSP) has a crucial role in the attempts of detecting supersymmetry (SUSY) since the lightest supersymmetric particle will escape the detectors unnoticed. The Large Hadron Collider (LHC) accelerates and collides mainly protons, and thus the collision processes are overwhelmed by the strong interactions. The superpartner of the top quark, stop, can be the lightest colored superpartner, mainly due to the splitting of the two stop scalar states amplified by the top Yukawa coupling.

In principle, the masses of the superpartners are free parameters in the minimal supersymmetric extension of the standard model (MSSM). The large number of the parameters parametrize the supersymmetry breaking, which is expected to be spontaneous in a more complete theory. The explicit SUSY breaking is introduced softly so that no quartic divergences re-appear. This requires inclusion of all the possible breaking terms, which are gauge invariant, into the Lagrangian. In models of a particular SUSY breaking mechanism, the number of parameters may be substantially smaller. Perhaps the most studied model is the constrained minimal supersymmetric standard model (CMSSM) [1, 2], which we also consider here. In CMSSM, supersymmetry is supposed to be broken spontaneously at the hidden sector by the SUSY breaking fields, which do not have gauge interactions with the SUSY fields that are, in principle, observable to us.

The breaking fields affect us through the gravitational strength interactions, which generate an effective Lagrangian with SUSY breaking terms. The effective Lagrangian does not have to be renormalizable anymore,

so it contains terms with couplings to the hidden sector fields suppressed by powers of inverse Planck mass. After the hidden sector fields generate vacuum expectation values, (renormalizable) soft SUSY breaking terms arise. This implies, under certain minimality assumptions, that the SUSY scalar terms have common couplings: the common scalar mass parameter  $m_0^2$ , a common bilinear parameter  $B_0$ , as well as a common trilinear parameter  $A_0$ , at the energy scale where the Lagrangian is established. This scale is thought to be the grand unification (GUT) scale.

Since the observations are made at the low energies, the renormalization group equations (RGE) must be used to calculate the running parameters, like the sparticle masses, at the low-energy scale. Even though the scalars have equal mass parameters at the GUT scale, this is not true at the electroweak (EW) scale anymore. Each scalar RGE has terms proportional to the corresponding fermionic partner Yukawa coupling. The effect of these terms is to decrease the mass parameter in question. Because of the large size of the top Yukawa coupling, the corresponding mass parameters entering to the stop mass matrix tend to decrease most, leading to the situation where the stops are the lightest squarks. The terms with gauge couplings have an opposite effect, as they appear with an opposite sign. Since the slepton mass parameter RGEs lack terms with the strong coupling constant, they do not increase as much as the squark mass parameters. Therefore, both the lighter stop and the lightest slepton, stau, are natural candidates for being the lightest supersymmetric scalar.

Supersymmetry by itself does not prevent the introduction of baryon and lepton number violating terms, which are not present in the standard model (SM) renormalizable Lagrangian. Such terms have a potential to lead to a very fast proton decay. Their presence is prevented by so-called  $R$ -parity [3]: SM particles are positively, and their superpartners, sparticles, negatively charged under this parity. The remarkable consequence is that the light-

\* [katri.huitu@helsinki.fi](mailto:katri.huitu@helsinki.fi)

† [lasse.leinonen@helsinki.fi](mailto:lasse.leinonen@helsinki.fi)

‡ [j.laamanen@science.ru.nl](mailto:j.laamanen@science.ru.nl)

est supersymmetric particle (LSP) must be absolutely stable. Therefore, a large number of LSPs may still be around from the early universe, which could explain the observed dark matter relic density (RD). In particle colliders, sparticles can be produced only in even numbers, since the initial state contains only ordinary particles. The LSP is thought to be uncharged (in both electric and color charges) which means that it may be only weakly interacting or that it only has gravitational interactions. Therefore, it is expected that it escapes the detectors unnoticed; only a missing energy component transverse to the colliding beam,  $E_T^{\text{miss}}$  (MET), is noticed.

The obvious candidate for the LSP in the MSSM spectrum is the lightest neutralino,  $\tilde{\chi}_1^0$ , which is the mixture of the neutral higgsinos, bino and wino, *i.e.* the superpartners of Higgs,  $B$  and  $W$ -bosons, respectively. Other candidates are the superpartner of graviton, gravitino, and superpartner of a neutrino, sneutrino. In gauge mediated supersymmetry breaking (GMSB) models [4], the LSP is always the gravitino, which is thus a natural dark matter candidate in these models. In GMSB, the leading contribution to the squark masses is proportional to the strong coupling constant, being larger than the leading contribution to the slepton masses. Thus, it is not expected that a strongly interacting particle is the NLSP in a minimal GMSB model. The searches at LEP collider exclude the possibility of light left-handed sneutrinos as the LSP, and masses beyond LEP's reach are ruled out by direct detection dark matter searches [5]. Unlike the partner of the left-handed neutrino, the partner of the right-handed neutrino is a viable dark matter candidate [6]. In such an extended model, also signatures of stop NLSP have been studied at the colliders [7].

In this paper, we study, within CMSSM, the possibility that the lighter stop scalar state is the NLSP. This, in particular, states that the lightest stop  $\tilde{t}_1$  is lighter than the lighter chargino ( $\tilde{\chi}_1^\pm$ ), the mixture of charged higgsinos and winos<sup>1</sup>. This also implies that the LSP is a neutralino<sup>2</sup>. This kind of a scenario requires large splitting between the two stop scalars. One consequence is that a wide gap opens in the sparticle mass spectrum between the scalars.  $\tilde{t}_1$  is the lonely scalar and close to the mass of  $\tilde{\chi}_1^0$  as a result of the relic density constraint. Therefore, stop is supposed to be the sparticle that is produced at the LHC in abundance. Stop NLSP in CMSSM with nonzero trilinear term has been studied, for example, in Refs. [11–13]. Implications at colliders have been studied, e.g., in Refs. [13–20]. In this work, we scan over all parameters and thus will comprehensively determine the possible regions of stop NLSP. We also map all the regions where dark matter constraints are met. Stop NLSP

may also arise in some compressed SUSY models [21, 22] or in the context of mirage mediation scenario [23, 24]. Light stop scenario is also favored in the view of the  $b-\tau$  Yukawa unification [25].

In section II, we discuss the conditions for stop being the NLSP and the decay modes of the stop NLSP. In section III, we list the constraints used in this paper. In section IV, we scan over relevant parameters to map the possible stop NLSP regions. In section V, we discuss the possibilities for detection of stop NLSP at the LHC, and we conclude in section VI.

## II. STOP AS AN NLSP

Stop can be the NLSP when the mixing term of the left- and right-labeled scalar states  $M_{LR}^2 = v(a_t \sin \beta - \mu y_t \cos \beta)$  in the stop mass matrix is large enough. The largest mixing occurs when the supersymmetric Higgs mass parameter  $\mu$  and the trilinear SUSY breaking parameter  $a_t$  have opposite signs. Here,  $y_t$  is the top Yukawa coupling,  $\beta$  is defined in the relation  $\tan \beta = v_2/v_1$ ,  $v_i$  being the vacuum expectation values of the two Higgs doublets obeying the relation  $v = \sqrt{v_1^2 + v_2^2}$ . We assume here that the trilinear soft parameters are proportional to the Yukawa couplings,  $a_i = y_i A_i$ , so the above mixing term can be written as  $M_{LR}^2 = m_t(A_t - \mu \cot \beta)$ .

In addition to the mixing, the renormalization group running plays an important role in the determination of the NLSP. In the scalar RGEs, the terms proportional to the Yukawa couplings (and the scalar masses) decrease the soft mass parameters, while the terms proportional to the gauge couplings (and gaugino masses) have an opposite effect. Because of the largeness of the strong coupling constant, the squark mass parameters tend to increase more than the slepton mass parameters, even though the third-generation squarks have large Yukawa couplings. Therefore, a small gaugino mass parameter as compared to the scalar mass parameter is preferred in order to suppress the strong coupling term in the squark RGE, which then may lead to a stop NLSP instead of stau NLSP.

The mass of the NLSP affects the relic density through co-annihilations. (The neutralino-stop co-annihilations were studied in Ref. [26].) Unless the annihilating LSPs are close to a resonance or are light, their annihilation usually cannot result in dark matter abundance within the observed limits. Rather, the relic density is usually too large. Co-annihilations with other particles, however, dilute the relic density, and with certain parameters, annihilations can even be too effective so that there is hardly any dark matter left after the annihilations cease. In the case of large (negative) values of  $A_t$ ,  $\mathcal{O}(\text{TeV})$ , and stop NLSP, the mass difference between stop and the neutralino LSP should not be less than 20 GeV or more than around 50 GeV in order to obtain the desired relic density, as we will show later (in the case of positive  $\mu$ ).

When stop is the NLSP and  $m_{\tilde{t}_1} - m_{\tilde{\chi}_1^0} < m_W$ , the

<sup>1</sup> In the anomaly mediated supersymmetry breaking (AMSB) models [8] chargino is the NLSP.

<sup>2</sup> The gravitino mass is not fixed in CMSSM, but the gravitino LSP with stop NLSP is not allowed [9]. In the so-called NUHM models [9, 10] stop can be the NLSP while gravitino is the LSP.

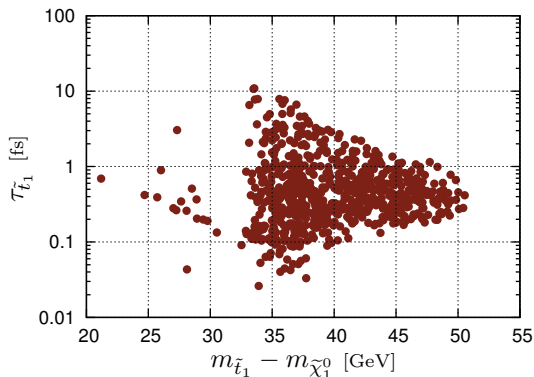


FIG. 1. Stop lifetime [fs] as a function of the NLSP-LSP mass difference. The points are the same RD=WMAP points as used later in Fig. 9.

only possible stop decays are

- $\tilde{t}_1 \rightarrow u\tilde{\chi}_1^0$
- $\tilde{t}_1 \rightarrow c\tilde{\chi}_1^0$
- $\tilde{t}_1 \rightarrow bf\tilde{f}'\tilde{\chi}_1^0$ .

Because of the required mass difference, the lifetime of stop is short, of the order of  $10^{-15}s$  (Fig. 1). The loop decay  $\tilde{t}_1 \rightarrow c\tilde{\chi}_1^0$  is enhanced by a large logarithm  $\ln(\Lambda_{\text{GUT}}^2/m_W^2)$ , and is likely to be dominant over the four-body decay, while smaller Cabibbo-Kobayashi-Maskawa (CKM) matrix elements suppress the other loop decay [27]. There are also scenarios where the four-body decay rate is at the same level or larger than the loop decay, for example when squark masses are not unified at a large mass scale, resulting only in a small logarithmic enhancement [28]. In section V, we will discuss the decay modes of stop when combined with the constraint requirements.

### III. CONSTRAINTS

In order to test the validity of a model, a number of constraints must be considered.

#### 1. The Higgs boson mass and other direct searches

The nonobservation of Higgs bosons and supersymmetric partners put stringent constraints on the parameters of SUSY models. The 95% C.L. exclusion limit for the SM Higgs boson mass of  $m_H > 114.4$  GeV [29] is applicable also to the lightest CP-even Higgs boson of the MSSM if it is SM-like. This implies that the Higgs coupling to the  $Z$  boson stays near to the SM value. If the  $hZZ$ -coupling is reduced, as may happen, e.g., at the large  $\tan\beta$ , a general SUSY Higgs mass bound,  $m_h > 92.8$  GeV, must be applied [29].

The light Higgs boson mass in SUSY models is generally sensitive to the higher-order corrections. Since there is a theoretical uncertainty of some 3 GeV from the next-to-next-to-leading order (NNLO) and higher corrections [30], a limit of  $m_h > 111$  is used in our calculations instead of the kinematic bound of 114.4 GeV. The SM-like  $Z$ -coupling is checked for this bound: A value  $\sin^2(\beta - \alpha_{eff}) > 0.9$  is required for the  $m_h > 111$  GeV limit in our work, otherwise, a limit  $m_h > 91$  GeV is used, which also leaves some room for theoretical uncertainties. Here,  $\alpha_{eff}$  is the effective mixing angle between neutral Higgs bosons.

The lightest Higgs boson mass is limited by  $m_Z$  at the tree level [31] even for more than two Higgs doublets [32]. The Higgs mass depends strongly on the  $\tan\beta$ , and a large  $\tan\beta$  is favored. The radiative corrections are crucial for bringing the light Higgs mass up to the acceptable level. The largest contributions typically come from the top and stop loops. In the decoupling regime ( $m_A \gg m_Z$  with  $\tan\beta \gg 1$ ), the leading 1-loop radiative correction to  $m_h^2$  can be written as  $m_h^2 = m_Z^2 + \epsilon_t + \epsilon_b$  [33], where

$$\epsilon_t = \frac{3m_t^4}{2\pi^2 v^2} \left( \ln \frac{M_S^2}{m_t^2} + \frac{X_t^2}{2M_S^2} - \frac{X_t^4}{12M_S^4} \right), \quad (3.1)$$

$$\epsilon_b = -\frac{3m_b^4}{2\pi^2 v^2} \frac{X_b^4}{12M_S^4}. \quad (3.2)$$

Here,  $M_S$  is a common soft SUSY-breaking mass term for the third-generation squarks and  $X_{t,b}$  are the mixing terms involving  $\mu$ ,  $\tan\beta$ , and the stop/sbottom trilinear couplings,

$$X_t = A_t - \mu \cot\beta, \quad (3.3)$$

$$X_b = A_b - \mu \tan\beta. \quad (3.4)$$

Because of the quartic dependence on the top mass, the  $\epsilon_t$  term is the leading one. In the maximal mixing scenario [34], the second and third terms of Eq. (3.1) cancel each other, leading to the mixing condition

$$X_t = \sqrt{6}M_S. \quad (3.5)$$

In the case of stop NLSP, the Higgs mass constraint seems to require nearly maximal mixing, as can be seen later.

Also, the other collider bounds from LEP, like chargino mass limits, and the LHC squark and gluino limits (CMS [35], ATLAS [36]) are important constraints. The LEP limits have been taken into account, as implemented in the program micrOmegas (v.2.4.R) [37]. The new LHC limits were also considered, where applicable.

#### 2. The $B \rightarrow \tau\nu$ decay

The final states of the decays of the type  $B \rightarrow l\nu$  consist purely on leptonic states, and the hadronic uncertainties are present only in the  $B$  meson decay constant

$f_B$ . Only the  $\tau$  channel has been observed so far. The SM expected value for the branching ratio, when using the value of  $|V_{ub}|$  given by the UTFit collaboration [38], is predicted to be [39]

$$\text{BR}(B^+ \rightarrow \tau^+ \nu_\tau)_{\text{SM}} = (0.80 \pm 0.15) \times 10^{-4}. \quad (3.6)$$

Recently, the experimental measurements from the  $B$ -factories have improved significantly, the most recent world average measurement being [40]

$$\text{BR}(B^+ \rightarrow \tau^+ \nu_\tau)_{\text{exp}} = (1.68 \pm 0.31) \times 10^{-4}. \quad (3.7)$$

The new physics (NP) contribution to the branching ratio can be quantified by defining a ratio [41]

$$R_{\tau\nu_\tau}^{\text{NP}} \equiv \frac{\text{BR}(B^+ \rightarrow \tau^+ \nu_\tau)_{\text{SM+NP}}}{\text{BR}(B^+ \rightarrow \tau^+ \nu_\tau)_{\text{SM}}}, \quad (3.8)$$

where the subscript SM+NP denotes the branching ratio of the NP scenario, including the SM contribution. The 95% C.L. allowed range for  $R_{\tau\nu_\tau}^{\text{NP}}$  is then [39]

$$0.99 < R_{\tau\nu_\tau}^{\text{NP}} < 3.19. \quad (3.9)$$

With higher-order corrections, the formula for the ratio is [41, 42]

$$R_{\tau\nu_\tau}^{\text{NP}} = \left( 1 - \frac{\tan^2 \beta}{1 + \tilde{\epsilon}_0 \tan \beta} \frac{m_B^2}{M_{H^\pm}^2} \right)^2, \quad (3.10)$$

where  $\tilde{\epsilon}_0$  contains all the higher-order corrections and  $m_B$  is the  $B$ -meson mass. The branching ratio depends strongly on the charged Higgs mass and  $\tan \beta$ , and typically the constraint (3.9) prefers small values of  $\tan \beta$  in order not to decrease the ratio too much below the lower limit (unless  $M_{H^\pm}$  is very light). A large charged Higgs mass decreases the new physics contributions in general.

### 3. The $(g-2)$ of muon

The anomalous magnetic moment of muon,  $a_\mu = (g-2)/2$  has been measured quite precisely a decade ago. The measured value [43] for  $a_\mu$  is

$$a_\mu^{\text{exp}} = (11659208.0 \pm 6.3) \times 10^{-10}. \quad (3.11)$$

The recent SM prediction for this is [44]

$$a_\mu^{\text{SM}} = (11659178.5 \pm 6.1) \times 10^{-10}. \quad (3.12)$$

leading to a discrepancy between the SM and experiment<sup>3</sup>,

$$\Delta a_\mu = (29.5 \pm 8.8) \times 10^{-10}. \quad (3.13)$$

This is a  $3.4 \sigma$  deviation. The SM prediction is largely dominated by leptonic QED processes, though careful calculation of hadronic and electroweak contributions is also necessary due to high precision of the experimental measurement. The hadronic processes, vacuum polarization above all, have more than an order of magnitude larger contribution to the magnetic moment compared to the electroweak processes.

Purely supersymmetric contribution of MSSM to  $a_\mu$  is proportional to  $\tan \beta \text{sign}(\mu)/M_{\text{SUSY}}^2$ , and for large enough  $\tan \beta$  and not too heavy supersymmetric particles, it can be larger than the electroweak contribution. For positive values of  $\mu$ , the MSSM can provide the solution to the discrepancy. For negative values of  $\mu$ , the new physics contributions drive the gap even wider. Because of this, a negative sign for  $\mu$  in the MSSM is usually considered to be disfavored [46].

As pointed out in [39], this constraint is complementary to the  $B \rightarrow \tau \nu$  decay constraint, and taken together, they rule out large areas of the parameter space.

The theoretical calculation of  $a_\mu$  is known to be difficult because of the hadronic contributions and nonperturbative effects involved, see *e.g.* [47–49] and references therein. Although there has been impressive improvements in the calculation, frequently the  $a_\mu$  constraint is not used in determining the excluded parameter space. We will take a similar attitude here, but comment on  $a_\mu$  when appropriate. When referring to this constraint, the following 95% C.L. limits, which include theoretical uncertainties, are used [50]:

$$1.15 \times 10^{-9} < \Delta a_\mu^{\text{SM+NP}} < 4.75 \times 10^{-9}. \quad (3.14)$$

Our acceptable parameter points have  $\Delta a_\mu^{\text{SM+NP}}$  below this range.

### 4. The $b \rightarrow s \gamma$ branching ratio

The present experimental value by the Heavy Flavor Averaging Group (HFAG) is [51]

$$\text{BR}(B \rightarrow X_s \gamma) = (355 \pm 24 \pm 9) \times 10^{-6}.$$

In our constraint, the theoretical uncertainties are included as well: in the SM at the NNLO QCD level the uncertainty can be estimated to be  $23 \times 10^{-6}$  [52], in the MSSM, the theoretical uncertainty is estimated to be additional 5% (we take  $15 \times 10^{-6}$ ) [53]. Combining all these gives (at  $2 \sigma$ )

$$\text{BR}(B \rightarrow X_s \gamma) = (355 \pm 142) \times 10^{-6}. \quad (3.15)$$

The  $b \rightarrow s \gamma$  constraint is sensitive to the sign of  $\mu$  [54], preferring the positive value.

### 5. Other constraints

The  $B_s \rightarrow \mu^+ \mu^-$  branching ratio can also be used as a constraint for new physics. The most recent experimental

<sup>3</sup> In a very recent paper [45] it was argued that the experimental and SM value actually agree.

upper limit by the CDF collaboration is [55]

$$BR(B_s \rightarrow \mu^+ \mu^-) < 4.3 \times 10^{-8} \text{ (95\% C.L.)} \quad (3.16)$$

Including the theoretical uncertainty from  $f_{B_s} = 238.8 \pm 9.5$  MeV [56], we find a conservative upper limit of

$$BR(B_s \rightarrow \mu^+ \mu^-) < 5.0 \times 10^{-8}. \quad (3.17)$$

In practice, this constraint is usually not the limiting factor, and in our calculations it is never the main constraint in otherwise good points. Therefore, we do not comment on this constraint further.

## 6. Relic density

Stable, (color and charge) neutral LSP provides a convenient candidate to explain the dark matter abundance observed by the Wilkinson Microwave Anisotropy Probe (WMAP) satellite mission. With the combined data from 7-year WMAP results, BAO (Baryon Acoustic Oscillations) in the distribution of galaxies, and observation of Hubble constant, the density of cold dark matter in the universe is determined to be [57]  $\Omega_c h^2 = 0.1126 \pm 0.0036$ . If 10 % theoretical uncertainty is added [58], we find the preferred WMAP range of

$$0.0941 < \Omega_c h^2 < 0.1311 \quad (3.18)$$

at  $2\sigma$  level. CMSSM can provide a dark matter density that is within the WMAP limits, at least in some parts of the parameter space. However, dark matter may be of nonsupersymmetric origin, so here we have used only the upper bound as a real constraint, unless otherwise indicated.

## IV. STOP NLSP PARAMETER SPACE

### A. Method

The CMSSM parameter space is in practice four-dimensional ( $m_0, M_{1/2}, A_0, \tan\beta$ ), with the sign ambiguity of the  $\mu$ -parameter doubling it. The actual value of the  $\mu$ -parameter is calculated from the radiative electroweak symmetry breaking (rEWSB) constraint condition [31, 59], which leaves the sign of  $\mu$  as a free parameter.  $M_{1/2}$  is the common gaugino mass, defined at the GUT scale by the boundary condition  $M_{1/2} = M_1 = M_2 = M_3$ , where  $M_{1,2,3}$  are the  $U(1)$ ,  $SU(2)$  and  $SU(3)$  gaugino masses, respectively. Limiting oneself to 2-dimensional parameter scans, on the one hand, reduces the effect of the other parameters to discrete examples, and on the other hand, creates easily an illusion of very restricted parameter space volume. Therefore, it is useful to actually explore the full parameter space. In order to find the parameter points, where stop is the NLSP and the experimental constraints are not violated, we scanned

the 4-dimensional parameter volume of the three GUT scale parameters and  $\tan\beta$  and calculated the low energy particle spectrum and the constraints for each point. The sign of  $\mu$  was chosen to be positive, partly guided by the preferences for some of the constraints of Sec. III. It should be noted that we restricted ourselves to the selection of real-valued parameters, which implies that no additional CP-violation is introduced by the soft SUSY breaking terms.

The particle spectrum was calculated using SOFT-SUSY (v.3.1.7) [60], and the relic density and constraints using micrOmegas (v.2.4.R) [37]. Top pole mass of  $m_t = 173.3$  GeV was used throughout this study.

### B. Stop NLSP regions

Figure 2 shows a 2-dimensional projection of the scanned 4-dimensional parameter space, where the ranges for parameters are (in [GeV],  $\mu > 0$ ):

$$\begin{aligned} 50 &\leq M_{1/2} \leq 1490|20; \\ 50 &\leq m_0 \leq 1990|20; \\ -5000 &\leq A_0 \leq 5000|100, \\ \tan\beta &\in \{2\dots7|1; 10\dots50|10\}. \end{aligned}$$

The number after ”|” denotes the stepping. Each point shows the identity of one of the possibly many potential NLSPs which results from varying the remaining two free parameters ( $\tan\beta$  and  $m_0$  in this case). The representative NLSP identity is chosen by keeping in mind that we would like to find all the points where stop can be the NLSP. Therefore, if a stop NLSP is found, it is chosen. Otherwise a stau,  $\tilde{\chi}_1^\pm$  or  $\tilde{\chi}_2^0$  NLSP is chosen, in that order of preference. Thus, an area labeled with  $\tilde{\tau}_1$  does not allow stop NLSPs for the scanned parameters, but may contain, e.g.,  $\tilde{\chi}_2^0$  NLSP. The rge-denoted (yellow) area shows the space where no combination of the parameters provides a good solution to the spectrum calculation (tachyons, no rEWSB ...). A large area of stop NLSP is found when the  $A_0$ -parameter is nonzero. With our choice of positive  $\mu$ , the negative  $A_0$ -parameter leads to larger mixing in stop mass matrix, see Eq. (3.3). Therefore, for a symmetric range, a larger number of potential stop NLSP points is found with negative  $A_0$ -parameters. A large  $\cot\beta$  is favored because of the enhancing effect in the stop mixing on the one hand, and because of the suppressing effect in the stau mixing on the other hand. Since  $\tan\beta$  is paired with the  $\mu$ -parameter, which is determined from the rEWSB condition, general upper or lower limits for  $\tan\beta$  are very involved. From our numerical calculations, however, we learn that the stop NLSP exists up to  $\tan\beta = 50$ , but for  $\tan\beta = 55$ , stau is the NLSP. For a large value of  $M_{1/2}$ , the upper value for  $\tan\beta$  drops to about 35 (stau being the NLSP otherwise). To have a better view of the stop NLSP points, we look at the negative  $A_0$ -parameters in more detail. We anticipate this also to alleviate the lightest Higgs boson mass limit

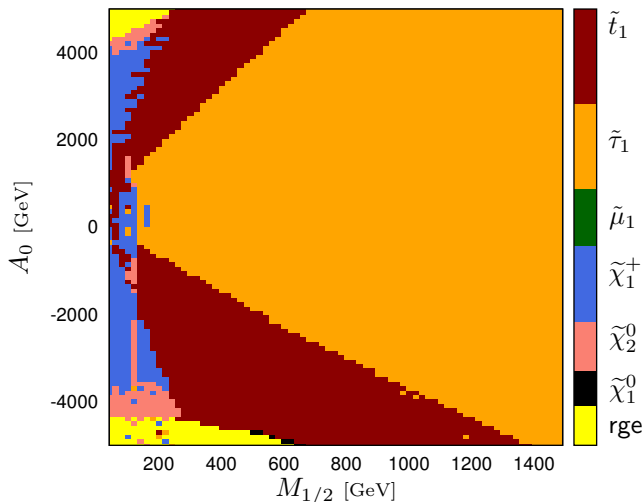


FIG. 2. The potential stop NLSP parameter space in dark brown (brown) on  $(M_{1/2}, A_0)$  plane. No constraints are applied yet.

constraint, as discussed in Sec. III 1. Some numerically unstable points may give erroneously large  $m_h$ , hence, we set also an upper limit for  $m_h$  to be 140 GeV [33, 61, 62], which cuts the unreliable points from the calculations.

In Fig. 3, the negative  $A_0$ -parameter space is plotted with respect to  $M_{1/2}$  as a 2-dimensional projection of the 4-dimensional parameter space showing the NLSP map. Parameters for subsequent figures are (in [GeV],  $\mu > 0$ ):

$$\begin{aligned} 100 &\leq M_{1/2} \leq 1800|20; \\ 1000 &\leq m_0 \leq 2848|66; \\ -8040 &\leq A_0 \leq -2200|80; \\ \tan \beta &\in \{2.5\dots 20|0.5; 25\dots 55|5\} \end{aligned}$$

A large space with stop NLSP is found. However, many of the potential stop-NLSP points conflict with the constraints specified earlier. The requirement of the neutralino relic density to fully explain the observed WMAP cold dark matter density is quite a restrictive constraint. This constraint may be weakened to the requirement that neutralino dark matter relic density should not exceed the upper WMAP limit for relic density. This, however, means that we cannot explain the dark matter puzzle with the SUSY model. Figure 3 shows, on top of the NLSP map, also scattered (red) points, where stop is the NLSP and the neutralino relic density is below the WMAP upper limit. The white subset of these points shows the parameters for which, in addition, the other constraints of Sec. III are not violated (however, excluding the muon magnetic moment, which is below the range (3.14)). In other words, these points are not excluded by the constraints discussed and exhibit the stop NLSP. When examined one by one, the  $\text{BR}(B^+ \rightarrow \tau^+ \nu_\tau)$  constraint limits the points only near the rge-denoted area, which is true also for the  $b \rightarrow s\gamma$  constraint. In contrast, the possible discrepancy in  $(g-2)_\mu$  cannot be explained with these models, since the calculated SUSY contribu-

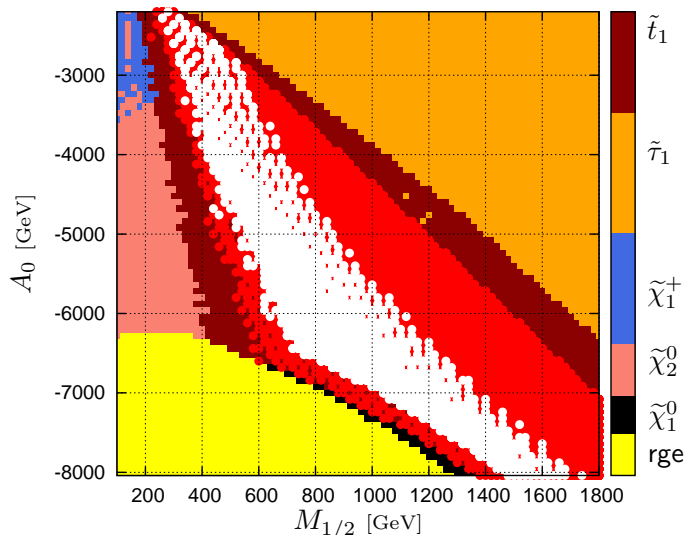


FIG. 3. The potential stop NLSP area in  $(M_{1/2}, A_0)$  plane. Zoomed from Fig. 2 to an interesting area. The red points are the stop NLSP points with relic density below the WMAP upper limit (which we denote from now on as  $\text{RD} \leq \text{WMAP}$ ), and the white subset of the points also obey the constraints of Sec. III. See the text.

tion here is always below the range of Eq. (3.14). When applying all the constraints (except  $(g-2)_\mu$ ) simultaneously, the white point area appears. It should be noted that there exists a subset of the above points, which nicely match the WMAP constraint, thus explaining also the amount of dark matter in the universe. Moreover, it matches the shown white dot area, just being sparser due to the limited number of scanned points. Therefore, it is possible to find points where stop is the NLSP, neutralino relic density matches the WMAP observation, and the collider constraints are fulfilled. This leaves still the possible deviation of the observed  $(g-2)_\mu$  unexplained. Even though the  $(g-2)_\mu$  value could be increased by considering the points with large  $\tan \beta$ , this conflicts with the  $\text{BR}(B^+ \rightarrow \tau^+ \nu_\tau)$  constraint. In addition,  $|A_0|$  should not be larger than 2–3 TeV for the  $(g-2)_\mu$  constraint to be fulfilled.  $(g-2)_\mu$  disfavors the stop-NLSP scenario. One may wonder if the large  $|A_0|$  values depicted can be physical, since typically charge and color-breaking minima occur for  $|A_0|$  much larger than  $m_0$  [63]. However, if the Universe is in a false vacuum, the tunneling probability to the real minimum can be very small [64]. We have checked for some examples with  $|A_0| \sim 7m_0$  that even if CCB minimum exists, the tunneling time scale is longer than the age of the Universe.

Figure 4 shows the equivalent of Fig. 3, but now the points are projected to  $(m_0, A_0)$ -plane. Figure 5 shows the projection to the  $(m_0, M_{1/2})$ -plane. In Video 1, the  $\tan \beta = 10$  slice of Fig. 5 is plotted. The points of Higgs maximal mixing (dark green) are distinguished from the other points that obey the relic density upper-limit constraint (red dots) and the points fulfilling also the other

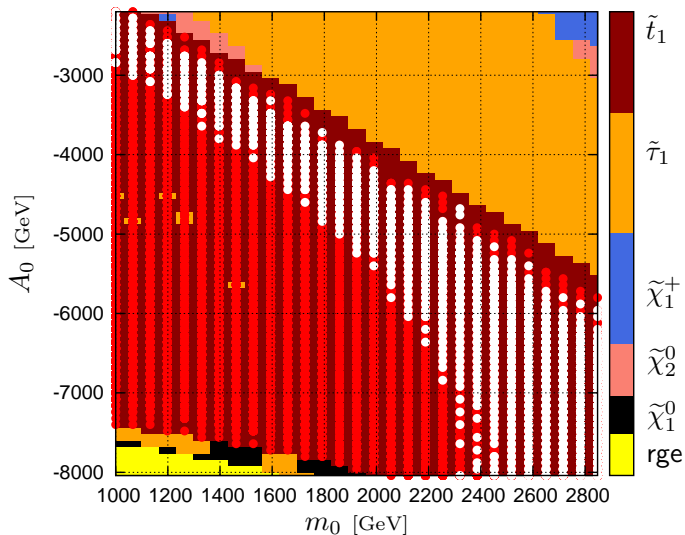


FIG. 4.  $RD \leq WMAP$ . Different projection.

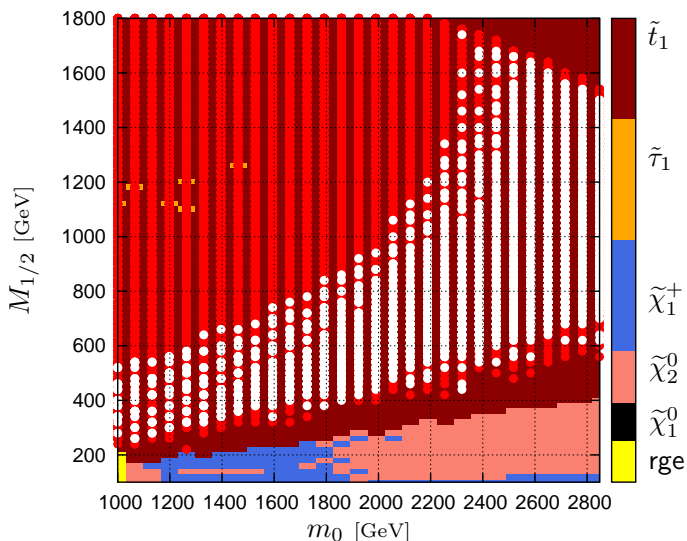
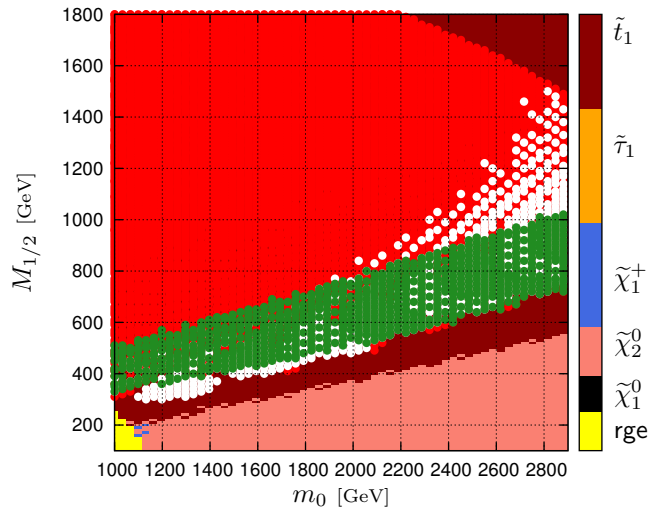


FIG. 5.  $RD \leq WMAP$ . Different projection.

constraints (white dots). The green points lie within 5% range from the optimal mixing value of Eq. (3.5). (See the animation of the evolution of the trilinear coupling from [65].) The maximal mixing coincides well with the good points, suggesting that the Higgs mass limit is, in fact, quite a severe constraint. The large area of sufficiently low relic density points (red) is generated, when the RGE conditions push the  $M_{1/2}$  parameter larger as the absolute value of the trilinear-parameter increases. This can be clearly seen in the video.

Figures 3–5 are different projections of the same parameter volume. It is interesting to see how the viewpoint exaggerates or understates certain aspects of the parameter space. For example, the area with no good spectrum (denoted by rge) seems to be quite large in Fig. 3, whereas in Fig. 5 it is hardly visible. An important message to be



Video 1. Points of optimal mixing (green) for stop NLSP points,  $\tan\beta = 10$ ,  $RD \leq WMAP$ . The scan is somewhat denser in this plot than in Fig. 5.

learned from this is that 2-dimensional extracts from a multidimensional parameter space may give a false feeling of the parameter space being very restricted.

### C. Masses

Searches for squarks and gluinos at the LHC disfavor a low mass region [35, 36]. If only stop is light, the anticipated exclusion limit would be lower than in the case of degenerate squarks and gluino due to smaller production cross section, and partly also due to  $t\bar{t}$  background. Also, proximity of the stop NLSP to the LSP might result in the supersymmetric events failing the missing energy cuts. A CMS search for jets+MET resulted in  $N_{max} = 13$  events at 95% confidence level for an integrated luminosity  $\mathcal{L} = 35 \text{ pb}^{-1}$ . The upper bound is related to the total SUSY production cross section by  $N_{max} = \epsilon \mathcal{L} \sigma_{max}$ . If we assume the total efficiency  $\epsilon$  to be 25% (e.g. see the discussion on efficiency in [35]), we can estimate the upper bound on the cross section to be  $\sigma_{max} = 1.5 \text{ pb}$ . Estimating that about one picobarn production cross section is needed to exclude a certain sparticle, we get for the lonely stop NLSP an anticipated lower mass limit of 300 GeV from  $t\bar{t}^*$  production using Prospino [66]. However, stop NLSP may not be easy to detect at the LHC, as will be discussed in the next section.

Interestingly, a small mass difference between stop and the LSP, and also a wide gap between the lighter stop and the other squarks are exactly what we find in the case of stop NLSP. Large splitting in the stop sector pushes lighter stop down to be a lonely SUSY scalar. The other scalars, except the light Higgs, are much heavier, with masses typically above 1 TeV. This is because the stop NLSP prefers large  $m_0$  as compared to  $M_{1/2}$  (about twice the  $M_{1/2}$  value in the following). In Fig. 6, a typical mass

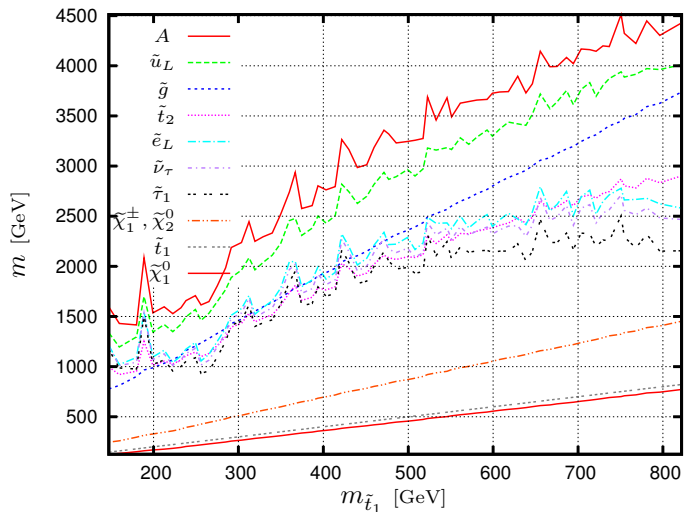


FIG. 6. Mass spectrum of a set of good stop NLSP points as a function of the stop mass. In the key, particles are listed in descending mass order found at  $m_{\tilde{t}_1} = 800$  GeV (RD=WMAP).

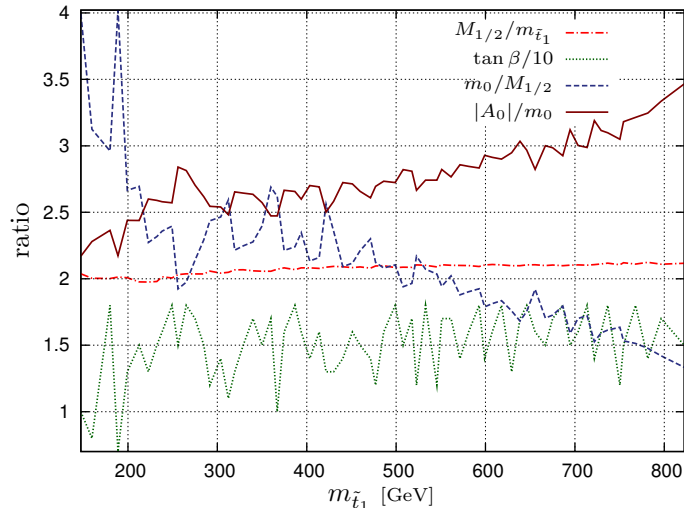


FIG. 7. Values of the parameters for Fig. 6

spectrum is plotted as a function of  $m_{\tilde{t}_1}$ . Only one stop and  $\tilde{\chi}_1^0$  are light, with masses close to each other. Each point in the plot is selected from the white points of the scan in Sec. IV B. The stop mass follows quite faithfully the  $M_{1/2}$  parameter, but the other parameters do not increase monotonically with the stop mass for the selected points. Therefore the neighboring points are not necessarily next to each other in the 4-dimensional parameter space. They, however, obey all the constraints except  $a_\mu$ , and were also required to explain the amount of dark matter (relic density is within the limits of Eq. (3.18), which we denote as RD=WMAP). In Fig. 7, we show the ratios of several parameters for the points in Fig. 6 (and consequently, for Figs. 10–13). In particular, it turns out that for these points,  $|A_0| < 3.5m_0$  always. The favored value of  $\tan \beta \sim 15$ . It is also clear that for heavier stops,

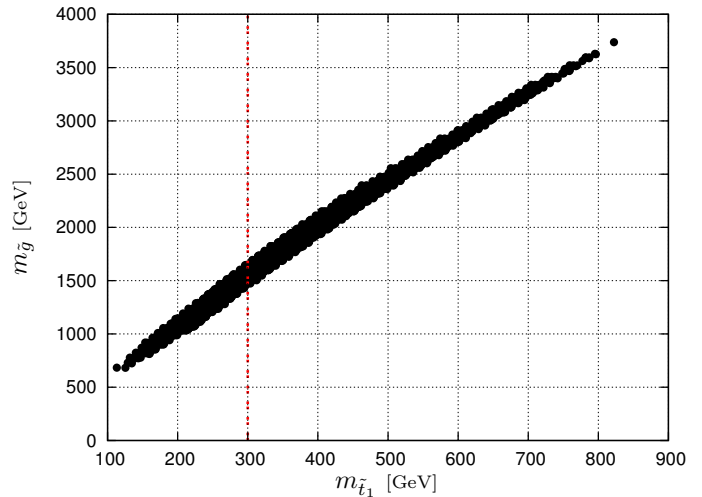


FIG. 8. Allowed points in  $(m_{\tilde{t}_1}, m_{\tilde{g}})$  plane, with stop NLSP, RD  $\leq$  WMAP. Vertical line reminds about the assumed LHC stop mass limit.

$m_0$  and  $M_{1/2}$  come closer to each other, while  $|A_0|$  value increases compared to  $m_0$ .

Figure 8 shows the allowed stop NLSP points in the  $(m_{\tilde{t}_1}, m_{\tilde{g}})$  plane for RD  $\leq$  WMAP. These points are the white points of the scan of Sec. IV B. There is a strong correlation with stop and gluino masses. If the stop NLSP mass is required to exceed 300 GeV, it would imply that the gluino mass is rather heavy. This is easily understood, since the LSP is a bino in a large part of the CMSSM parameter space. The relic density constraint requires the stop mass therefore to be rather close to the  $\tilde{\chi}_1^0$  mass, so that co-annihilations are able to dilute the excess LSP density. The gaugino mass relation  $M_1 : M_2 : M_3 \simeq 1 : 1.9 : 6.2$  at the EW-scale [24] then predicts the gluino mass to be about 5–6 times the stop mass ( $m_{\tilde{g}} \approx 6.2 \times M_1$ , and  $m_{\tilde{t}_1} = m_{LSP} + 10\% = 1.10 \times M_1$ , hence  $m_{\tilde{g}}/m_{\tilde{t}_1} \approx 5.5$ ).

In Fig. 9, the mass difference of NLSP-stop and  $\tilde{\chi}_1^0$  is plotted with respect to the stop mass for the same allowed stop NLSP points. The mass difference seems to be typically below approximately 50 GeV. This is a consequence of the relic density constraint, which requires effective co-annihilations for the bino LSP. (The exact WMAP preferred region saturates the upper edge of the mass range, see Fig. 9.) Another implication is that the stop decay channels are limited to the ones explained in Sec. II.

## V. STOP NLSP AT THE LHC

In the stop NLSP case, it is quite possible that most of the supersymmetric partners are relatively heavy as discussed in the previous section. Discovering stop has been studied in detail in several works, *e.g.*, in [13–20, 67, 68]. Here, we will shortly discuss the cross sections

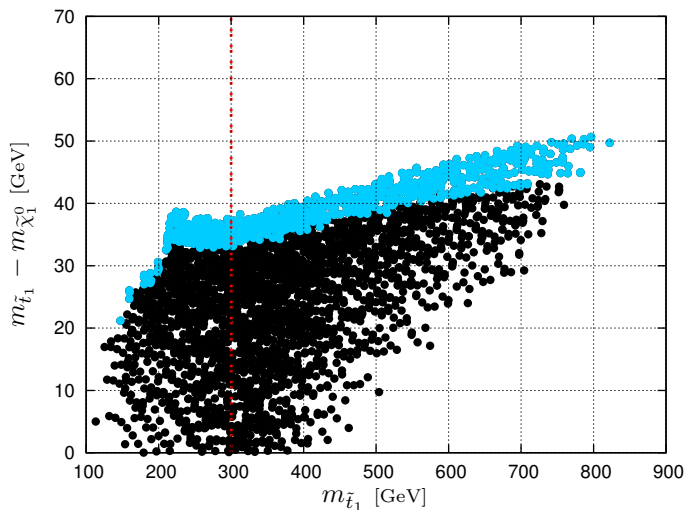


FIG. 9. Mass difference of the two lightest SUSY particles wrt.  $m_{\tilde{t}_1}$ , for black dots RD < WMAP and for light blue dots RD=WMAP. Vertical line reminds about the assumed LHC stop mass limit.

$\sigma(pp \rightarrow \tilde{x}\tilde{y})$	7 TeV	14 TeV
$\tilde{t}_1\tilde{t}_1^*$	1130	9240
$\tilde{g}\tilde{q}$	$0.958 \times 10^{-1}$	30.2
$\tilde{\chi}_2^0\tilde{\chi}_1^+$	3.36	21.5
$\tilde{g}\tilde{g}$	$0.634 \times 10^{-1}$	15.7
$\tilde{\chi}_1^+\tilde{\chi}_1^-$	2.05	14.9
$\tilde{q}\tilde{q}$	$0.184 \times 10^{-1}$	9.48
$\tilde{\chi}_2^0\tilde{g}$	$0.136 \times 10^{-1}$	0.679
$\tilde{\chi}_1^+\tilde{q}$	$0.969 \times 10^{-2}$	0.639
$\tilde{\chi}_2^0\tilde{q}$	$0.635 \times 10^{-2}$	0.452

TABLE I. Cross sections [fb] at the LHC for  $M_{1/2} = 620$  GeV,  $m_0 = 1528$  GeV,  $A_0 = -3880$  GeV,  $\tan\beta = 14$ , and  $\text{sign}(\mu) = +1$ , corresponding to  $m_{\tilde{t}_1} = 304$  GeV of Fig. 6 (Prospino2, NLO).

and decay modes of stop NLSP at the LHC, when the constraints discussed in previous sections are fulfilled.

Typically, the  $\tilde{t}_1\tilde{t}_1^*$  cross section is very large compared to the other production mechanisms via cascade decays of other sparticles. For example, in Table I, the next-to-leading order LHC cross sections for several squark and gaugino production channels are calculated for one acceptable parameter point corresponding to  $m_{\tilde{t}_1} = 304$  GeV of Fig. 6.

In Fig. 10, we have plotted the dominant decay modes of the lightest stop as a function of its mass for the points in Fig. 6. The dominant decay mode is through  $\tilde{\chi}_1^0 c$  channel, but the importance of  $bf\tilde{f}'\tilde{\chi}_1^0$  channel increases with increasing stop mass and the mass difference to the LSP (Fig. 9). In Fig. 11, the branching ratios of gluino are plotted as a function of its mass for the same points. Gluino decays dominantly to a stop-top pair. The charge conjugated mode is also included in

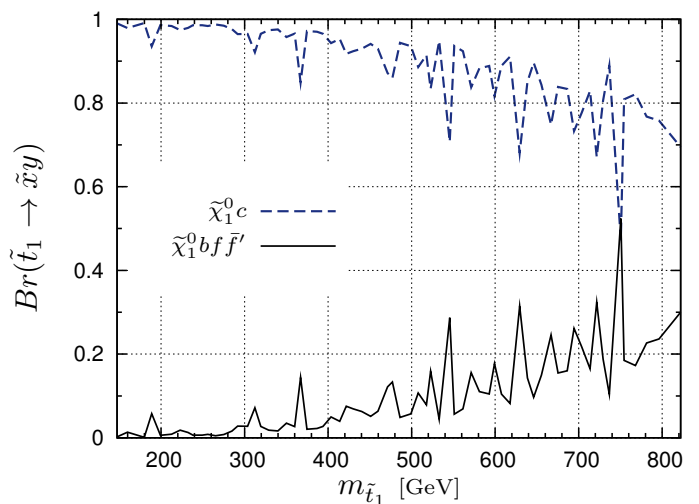


FIG. 10. Branching ratios of lightest stop for the collection of allowed points, RD = WMAP.

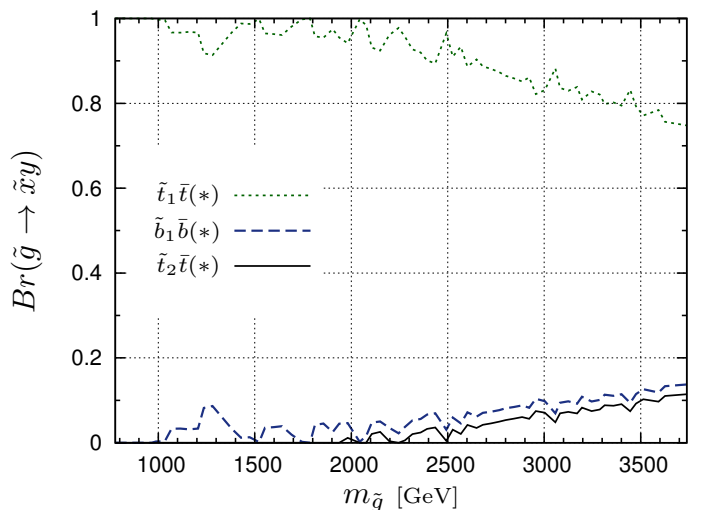


FIG. 11. Branching ratios of gluino for the collection of allowed points, RD = WMAP. (\*) indicates that the charge conjugate state is also included.

the plotted value. For the evaluation of branching ratios and the decays of the supersymmetric particles, we have used SUSY-HIT (v.1.3 with SDECAY v1.3b/HDECAY v3.4) [69]. It should be noted, though, that the approximate result for the  $\tilde{t}_1 \rightarrow \tilde{\chi}_1^0 c$  decay used in [69] has to be taken with care in case the minimal flavor violation scale is not large and has to be reanalyzed more carefully [70]. The cross sections have been calculated to next-to-leading order (NLO) using Prospino2 (v."on\_the\_web\_11\_3\_10") [66].

In Fig. 12, the LHC 14 TeV cross section for the like-sign top process  $pp \rightarrow \tilde{g}\tilde{g} \rightarrow \tilde{\chi}_1^0\tilde{\chi}_1^0\tilde{c}\tilde{t}\tilde{t}/\tilde{\chi}_1^0\tilde{\chi}_1^0\tilde{t}\tilde{t}cc$  [pb] has been plotted as a function of stop mass up to 400 GeV, where the cross section is already hopelessly small. The points correspond to the previously used stop NLSP set,

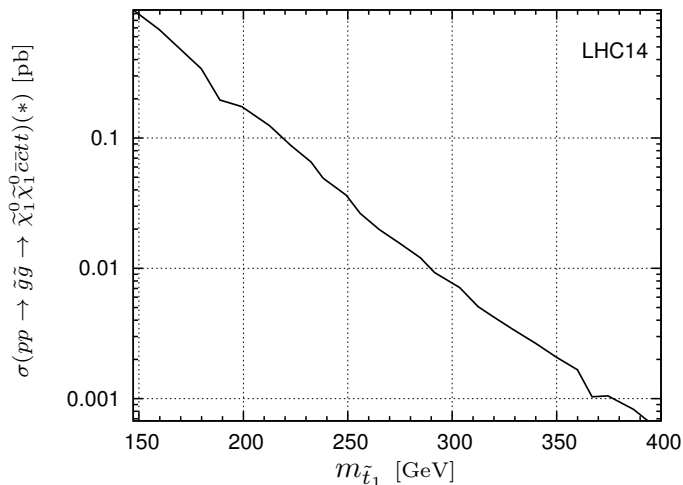


FIG. 12. Cross section of the process  $pp \rightarrow \tilde{g}\tilde{g} \rightarrow \tilde{\chi}_1^0 \tilde{\chi}_1^0 c\bar{c}t\bar{t} (*)$  [pb], for collection of allowed points, RD = WMAP. The final state includes both combinations of like-sign tops.

which passes the constraints (points in Figs. 6, 10, 11). The plotted cross section contains contributions from both charge conjugation final states. For  $m_{\tilde{t}_1} = 300$  GeV, the cross section is around 10 fb but decreases fast with increasing stop mass, which is caused by the declining gluino production cross section. The background of like-sign decays can be removed [18], which makes the process interesting for probing light stops at the LHC.

The stop pair production cross section is clearly the largest production channel. However, for a light stop, the loop decay dominates, and the final state of almost back-to-back neutralinos and two soft  $c$ -jets is not experimentally promising. For heavier stops, the four-body branching ratio competes with the loop decay one. In Fig. 13, the LHC 14 TeV cross section for the process  $pp \rightarrow \tilde{t}_1 \tilde{t}_1^* \rightarrow (\tilde{\chi}_1^0 b f \bar{f}') (\tilde{\chi}_1^0 \bar{c}) + \text{charge conjugated final state}$  [pb] has been plotted for the same stop NLSP set, which passes the constraints (the middle curve). The cross section remains reasonably large,  $\mathcal{O}(10 \text{ fb})$ , even for  $m_{\tilde{t}_1} \sim 800$  GeV. When the fermions  $ff'$  are  $\ell\nu$  from  $W$ , the signal would be a  $b$ -jet and charged lepton in one hemisphere and missing energy from neutralinos, neutrinos, and a soft  $c$ -jet in the other hemisphere. A detailed signal analysis is not the purpose of this work, but this signature may be possible. The cross section where both stops decay to four particles is for all studied stop masses around  $\mathcal{O}(10 \text{ fb})$ , although the variation between neighboring points may be large.

## VI. SUMMARY AND DISCUSSION

We have studied the interesting possibility of stop being the next-to-lightest supersymmetric particle within the CMSSM scenario. Large mixing in the stop mass matrix can result in a (relatively) light stop squark, and in some cases, it can be the NLSP. Typically this prefers

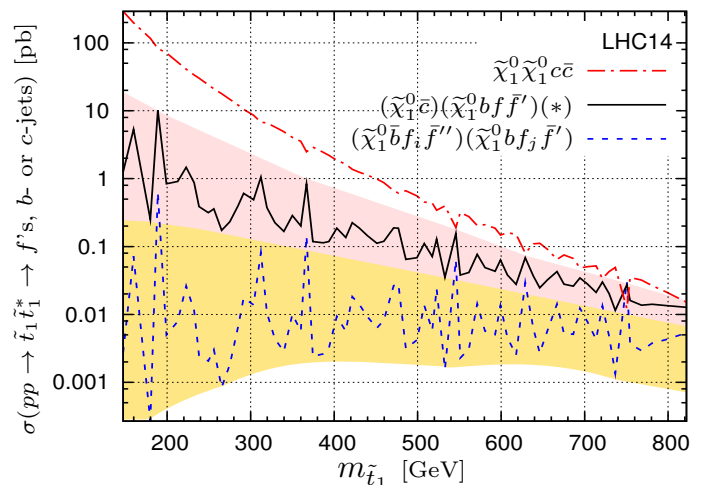


FIG. 13. Cross section of the process  $pp \rightarrow \tilde{t}_1 \tilde{t}_1^* \rightarrow \tilde{\chi}_1^0 \tilde{\chi}_1^0 c\bar{c}$  [pb] (upper), the process  $pp \rightarrow \tilde{t}_1 \tilde{t}_1^* \rightarrow (\tilde{\chi}_1^0 \bar{c})(\tilde{\chi}_1^0 b f \bar{f}') + \text{charge conjugated final state}$  [pb] (in the middle, including the charge conjugated final state), and the process  $pp \rightarrow \tilde{t}_1 \tilde{t}_1^* \rightarrow (\tilde{\chi}_1^0 \bar{b} f_i \bar{f}_i') (\tilde{\chi}_1^0 b f_j \bar{f}_j')$  [pb] (the lowest), for collection of allowed points, RD = WMAP.

a large nonzero value for the trilinear mass parameter  $A_t$ . In addition, a large  $\mu$ -parameter naturally splits the stop pair, and may also result in a light  $m_{\tilde{t}_1}$ , unless there is cancellation between  $\mu$  and  $A_t$ . Large parameter spaces with the lighter stop as an NLSP can be found, which simultaneously fulfill various experimental constraints. Within these regions, the neutralino LSP may explain the dark matter problem. The  $\text{BR}(B^+ \rightarrow \tau^+ \nu_\tau)$ ,  $\text{BR}(B \rightarrow X_s \gamma)$  and  $\text{BR}(B_s \rightarrow \mu^+ \mu^-)$  constraints agree with the experimental limits, but we have not found points where the possibly large observed discrepancy of  $(g-2)_\mu$  from the SM expected value could be explained. The CP-even Higgs boson lower mass limit is a severe constraint, which many times rules otherwise good parameter spaces out.

The LHC is currently pushing squark and gluino lower mass limits to higher values. The nonobservation of sparticles may fit to the scenario, where the NLSP is a rather heavy squark. In CMSSM, this would in most cases be the lighter stop squark. We have argued that observing the top signal resulting from this scenario is quite challenging. The like-sign top channel, that relies on the Majorana character of the gluinos, requires reasonably large production cross section of gluinos at the LHC. In the stop NLSP scenario with, let us say, heavier than 350 GeV stop, the gluino is very heavy, about five times that, by the WMAP constraint and gaugino mass ratios. Therefore, the gluino production will be scant, resulting in the like-sign top signal to lie in a subfemtobarn range. Because of the relative lightness of stop with respect to the other SUSY scalars, their direct pair production dominates. In the case of heavy stop NLSP, the production and decay chain  $pp \rightarrow \tilde{t}_1 \tilde{t}_1^* \rightarrow b\ell\nu + \cancel{E}_T$  may be possible (see also [68]). Alternatively to the stop production alone, signals where other particles are used in order to

discover stops can be utilized, as studied, *e.g.*, in [15] for light stops.

## VII. ACKNOWLEDGMENTS

We thank Ritva Kinnunen for discussions, and Debajyoti Choudhury for participating in the early stage of the investigation. We thank Nordita program *TeV Scale Physics and Dark Matter* for hospitality while this work was being initiated. KH and LL acknowledge support from the Academy of Finland (Project No. 137960). The work of JL is supported by the Foundation for Fundamental Research of Matter (FOM). LL thanks Magnus Ehrnrooth Foundation for financial support.

- 
- [1] A. H. Chamseddine, R. L. Arnowitt, and P. Nath, *Phys. Rev. Lett.* **49**, 970 (1982).
- [2] G. L. Kane, C. F. Kolda, L. Roszkowski, and J. D. Wells, *Phys. Rev.* **D49**, 6173 (1994), [arXiv:hep-ph/9312272](#).
- [3] A. Salam and J. A. Strathdee, *Nucl. Phys.* **B87**, 85 (1975); P. Fayet, *ibid.* **B90**, 104 (1975); G. R. Farrar and P. Fayet, *Phys. Lett.* **B76**, 575 (1978); S. Dimopoulos, S. Raby, and F. Wilczek, *ibid.* **B112**, 133 (1982); G. R. Farrar and S. Weinberg, *Phys. Rev.* **D27**, 2732 (1983).
- [4] M. Dine and A. E. Nelson, *Phys.Rev.* **D48**, 1277 (1993), [arXiv:hep-ph/9303230 \[hep-ph\]](#); M. Dine, A. E. Nelson, and Y. Shirman, *ibid.* **D51**, 1362 (1995), [arXiv:hep-ph/9408384 \[hep-ph\]](#); M. Dine, A. E. Nelson, Y. Nir, and Y. Shirman, *ibid.* **D53**, 2658 (1996), [arXiv:hep-ph/9507378 \[hep-ph\]](#).
- [5] D. O. Caldwell, R. Eisberg, D. Grumm, M. S. Witherell, B. Sadoulet, *et al.*, *Phys.Rev.Lett.* **61**, 510 (1988), revision of UCSB-HEP-87-13; D. O. Caldwell, B. Magnusson, M. S. Witherell, A. Da Silva, B. Sadoulet, *et al.*, *ibid.* **65**, 1305 (1990); D. Reusser, M. Treichel, F. Boehm, C. Brogini, P. Fisher, *et al.*, *Phys.Lett.* **B255**, 143 (1991); M. Mori *et al.* (KAMIOKANDE Collaboration), *Phys.Rev.* **D48**, 5505 (1993).
- [6] T. Asaka, K. Ishiwata, and T. Moroi, *Phys. Rev.* **D73**, 051301 (2006), [arXiv:hep-ph/0512118](#); **D75**, 065001 (2007), [arXiv:hep-ph/0612211](#).
- [7] A. de Gouvea, S. Gopalakrishna, and W. Porod, *JHEP* **11**, 050 (2006), [arXiv:hep-ph/0606296](#); D. Choudhury, S. K. Gupta, and B. Mukhopadhyaya, *Phys.Rev.* **D78**, 015023 (2008), [arXiv:0804.3560 \[hep-ph\]](#).
- [8] L. Randall and R. Sundrum, *Nucl.Phys.* **B557**, 79 (1999), [arXiv:hep-th/9810155 \[hep-th\]](#); G. F. Giudice, M. A. Luty, H. Murayama, and R. Rattazzi, *JHEP* **9812**, 027 (1998), [arXiv:hep-ph/9810442 \[hep-ph\]](#); T. Gherghetta, G. F. Giudice, and J. D. Wells, *Nucl. Phys.* **B559**, 27 (1999), [arXiv:hep-ph/9904378](#); A. Pomarol and R. Rattazzi, *JHEP* **05**, 013 (1999), [arXiv:hep-ph/9903448](#).
- [9] J. L. Diaz-Cruz, J. R. Ellis, K. A. Olive, and Y. Santoso, *JHEP* **05**, 003 (2007), [arXiv:hep-ph/0701229](#).
- [10] H. Baer, A. Mustafayev, S. Profumo, A. Belyaev, and X. Tata, *JHEP* **0507**, 065 (2005), [arXiv:hep-ph/0504001 \[hep-ph\]](#).
- [11] U. Chattopadhyay, D. Das, A. Datta, and S. Poddar, *Phys.Rev.* **D76**, 055008 (2007), [arXiv:0705.0921 \[hep-ph\]](#).
- [12] A. Gladyshev, D. Kazakov, and M. Paucar(2007), [arXiv:0704.1429 \[hep-ph\]](#).
- [13] S. P. Das, A. Datta, and M. Guchait, *Phys.Rev.* **D65**, 095006 (2002), [arXiv:hep-ph/0112182 \[hep-ph\]](#).
- [14] N. Bhattacharyya, A. Datta, and M. Maity, *Phys. Lett.* **B669**, 311 (2008), [arXiv:0807.0994 \[hep-ph\]](#).
- [15] S. Bornhauser, M. Drees, S. Grab, and J. S. Kim, *Phys. Rev.* **D83**, 035008 (2011), [arXiv:1011.5508 \[hep-ph\]](#).
- [16] M. Johansen, J. Edsjo, S. Hellman, and D. Milstead, *JHEP* **1008**, 005 (2010), [arXiv:1003.4540 \[hep-ph\]](#).
- [17] G. Hiller, J. S. Kim, and H. Sedello, *Phys.Rev.* **D80**, 115016 (2009), [arXiv:0910.2124 \[hep-ph\]](#).
- [18] S. Kraml and A. Raklev, *Phys.Rev.* **D73**, 075002 (2006), [arXiv:hep-ph/0512284 \[hep-ph\]](#).
- [19] K. A. Olive and S. Rudaz, *Phys.Lett.* **B340**, 74 (1994), [arXiv:hep-ph/9408280 \[hep-ph\]](#).
- [20] R. Demina, J. D. Lykken, K. T. Matchev, and A. Nomerotski, *Phys. Rev.* **D62**, 035011 (2000), [arXiv:hep-ph/9910275](#).
- [21] S. P. Martin, *Phys.Rev.* **D75**, 115005 (2007), [arXiv:hep-ph/0703097 \[HEP-PH\]](#); **D78**, 055019 (2008), [arXiv:0807.2820 \[hep-ph\]](#).
- [22] H. Baer, A. Box, E.-K. Park, and X. Tata, *JHEP* **0708**, 060 (2007), [arXiv:0707.0618 \[hep-ph\]](#).
- [23] K. Choi, K. S. Jeong, and K.-i. Okumura, *JHEP* **0509**, 039 (2005), [arXiv:hep-ph/0504037 \[hep-ph\]](#); O. Loaiza-Brito, J. Martin, H. P. Nilles, and M. Ratz, *AIP Conf.Proc.* **805**, 198 (2006), [arXiv:hep-th/0509158 \[hep-th\]](#); K. Choi, K. Y. Lee, Y. Shimizu, Y. G. Kim, and K.-i. Okumura, *JCAP* **0612**, 017 (2006), [arXiv:hep-ph/0609132 \[hep-ph\]](#).
- [24] K. Huitu, J. Laamanen, P. Pandita, and P. Tiitola, *Phys.Rev.* **D82**, 115003 (2010), [arXiv:1006.0661 \[hep-ph\]](#).
- [25] I. Gogoladze, S. Raza, and Q. Shafi(2011), [arXiv:1104.3566 \[hep-ph\]](#).
- [26] J. R. Ellis, K. A. Olive, and Y. Santoso, *Astropart.Phys.* **18**, 395 (2003), [arXiv:hep-ph/0112113 \[hep-ph\]](#).
- [27] K.-I. Hikasa and M. Kobayashi, *Phys.Rev.* **D36**, 724 (1987).
- [28] C. Boehm, A. Djouadi, and Y. Mambrini, *Phys.Rev.* **D61**, 095006 (2000), [arXiv:hep-ph/9907428 \[hep-ph\]](#).
- [29] K. Nakamura *et al.* (Particle Data Group), *J.Phys.G* **G37**, 075021 (2010).
- [30] G. Degrossi, S. Heinemeyer, W. Hollik, P. Slavich, and G. Weiglein, *Eur.Phys.J.* **C28**, 133 (2003), [arXiv:hep-ph/0212020 \[hep-ph\]](#); S. Heinemeyer, *Int.J.Mod.Phys.* **A21**, 2659 (2006), [arXiv:hep-ph/0407244 \[hep-ph\]](#).

- [31] K. Inoue, A. Kakuto, H. Komatsu, and S. Takeshita, *Prog.Theor.Phys.* **67**, 1889 (1982), revised version.
- [32] R. A. Flores and M. Sher, *Annals Phys.* **148**, 95 (1983).
- [33] B. Allanach, A. Djouadi, J. Kneur, W. Porod, and P. Slavich, *JHEP* **0409**, 044 (2004), [arXiv:hep-ph/0406166 \[hep-ph\]](#).
- [34] M. S. Carena, S. Heinemeyer, C. Wagner, and G. Weiglein(1999), [arXiv:hep-ph/9912223 \[hep-ph\]](#).
- [35] V. Khachatryan *et al.* (CMS), *Phys. Lett.* **B698**, 196 (2011), [arXiv:1101.1628 \[hep-ex\]](#).
- [36] G. Aad *et al.* (Atlas Collaboration), *Phys.Lett.* **B701**, 186 (2011), [arXiv:1102.5290 \[hep-ex\]](#).
- [37] G. Belanger, F. Boudjema, A. Pukhov, and A. Semenov, *Comput.Phys.Commun.* **176**, 367 (2007), [arXiv:hep-ph/0607059 \[hep-ph\]](#).
- [38] M. Bona *et al.* (UTfit Collaboration), *Phys.Lett.* **B687**, 61 (2010), [arXiv:0908.3470 \[hep-ph\]](#).
- [39] B. Bhattacharjee, A. Dighe, D. Ghosh, and S. Raychaudhuri, *Phys.Rev.* **D83**, 094026 (2011), [arXiv:1012.1052 \[hep-ph\]](#).
- [40] S. T’Jampens (CKMfitter Collaboration), “From the KM ansatz to the search of new physics in  $\Delta F=2$  FCNC,” (2010), conference talk at ICHEP, <http://indico.cern.ch/getFile.py/access?contribId=190&sessionId=53&resId=0&materialId=slides&confId=73513>.
- [41] G. Isidori and P. Paradisi, *Phys.Lett.* **B639**, 499 (2006), [arXiv:hep-ph/0605012 \[hep-ph\]](#).
- [42] A. Akeroyd and S. Recksiegel, *J.Phys.G* **G29**, 2311 (2003), [arXiv:hep-ph/0306037 \[hep-ph\]](#).
- [43] G. Bennett *et al.* (Muon G-2 Collaboration), *Phys.Rev.* **D73**, 072003 (2006), [arXiv:hep-ex/0602035 \[hep-ex\]](#).
- [44] J. P. Miller, E. de Rafael, and B. Roberts, *Rept.Prog.Phys.* **70**, 795 (2007), [arXiv:hep-ph/0703049 \[hep-ph\]](#).
- [45] S. Bodenstein, C. A. Dominguez, and K. Schilcher(2011), [arXiv:1106.0427 \[hep-ph\]](#).
- [46] D. Stockinger, *J.Phys.G* **G34**, R45 (2007), [arXiv:hep-ph/0609168 \[hep-ph\]](#).
- [47] M. Knecht, *Lect. Notes Phys.* **629**, 37 (2004), [arXiv:hep-ph/0307239](#).
- [48] J. Prades, *Acta Phys. Polon. Supp.* **3**, 75 (2010), [arXiv:0909.2546](#).
- [49] K. Hagiwara, R. Liao, A. D. Martin, D. Nomura, and T. Teubner, *J.Phys.G* **G38**, 085003 (2011), [arXiv:1105.3149 \[hep-ph\]](#).
- [50] D. Eriksson, F. Mahmoudi, and O. Stal, *JHEP* **11**, 035 (2008), [arXiv:0808.3551 \[hep-ph\]](#).
- [51] D. Asner *et al.* (Heavy Flavor Averaging Group)(2010), [arXiv:1010.1589 \[hep-ex\]](#).
- [52] M. Misiak, H. Asatrian, K. Bieri, M. Czakon, A. Czarnecki, *et al.*, *Phys.Rev.Lett.* **98**, 022002 (2007), [arXiv:hep-ph/0609232 \[hep-ph\]](#).
- [53] J. R. Ellis, S. Heinemeyer, K. A. Olive, A. M. Weber, and G. Weiglein, *JHEP* **08**, 083 (2007), [arXiv:0706.0652 \[hep-ph\]](#).
- [54] P. Nath and R. L. Arnowitt, *Phys.Lett.* **B336**, 395 (1994), [arXiv:hep-ph/9406389 \[hep-ph\]](#).
- [55] D. Glenzinski *et al.* (CDF), “Search for the Rare Decays  $B_s(d) \rightarrow \mu + \mu^-$ ,” CDF public note 9892, [http://www-cdf.fnal.gov/physics/new/bottom/090813\\_blessed-Bsd2mumu//bsmumupub3.7fb\\_v01.pdf](http://www-cdf.fnal.gov/physics/new/bottom/090813_blessed-Bsd2mumu//bsmumupub3.7fb_v01.pdf).
- [56] J. Laiho, E. Lunghi, and R. S. Van de Water, *Phys. Rev.* **D81**, 034503 (2010), [arXiv:0910.2928 \[hep-ph\]](#).
- [57] E. Komatsu *et al.* (WMAP Collaboration), *Astrophys.J.Suppl.* **192**, 18 (2011), [arXiv:1001.4538 \[astro-ph.CO\]](#).
- [58] N. Baro, F. Boudjema, and A. Semenov, *Phys. Lett.* **B660**, 550 (2008), [arXiv:0710.1821 \[hep-ph\]](#).
- [59] L. E. Ibanez and G. G. Ross, *Phys.Lett.* **B110**, 215 (1982); L. Alvarez-Gaume, J. Polchinski, and M. B. Wise, *Nucl.Phys.* **B221**, 495 (1983), revised version; J. R. Ellis, D. V. Nanopoulos, and K. Tamvakis, *Phys.Lett.* **B121**, 123 (1983).
- [60] B. Allanach, *Comput.Phys.Commun.* **143**, 305 (2002), [arXiv:hep-ph/0104145 \[hep-ph\]](#).
- [61] G. L. Kane, C. F. Kolda, and J. D. Wells, *Phys. Rev. Lett.* **70**, 2686 (1993), [arXiv:hep-ph/9210242](#).
- [62] J. R. Espinosa and M. Quiros, *Phys. Lett.* **B302**, 51 (1993), [arXiv:hep-ph/9212305](#).
- [63] J. Casas, A. Lleyda, and C. Munoz, *Nucl.Phys.* **B471**, 3 (1996), [arXiv:hep-ph/9507294 \[hep-ph\]](#).
- [64] A. Kusenko, P. Langacker, and G. Segre, *Phys.Rev.* **D54**, 5824 (1996), [arXiv:hep-ph/9602414 \[hep-ph\]](#).
- [65] “Animation of the parameter space evolution,” <http://www.youtube.com/watch?v=vyizA4262Qg> (2011), [Video on Youtube by the present authors].
- [66] W. Beenakker, R. Hopker, and M. Spira(1996), Prospino2, [arXiv:hep-ph/9611232 \[hep-ph\]](#), <http://www.thphys.uni-heidelberg.de/~plehn/prospino>; W. Beenakker, M. Kramer, T. Plehn, M. Spira, and P. M. Zerwas, *Nucl. Phys.* **B515**, 3 (1998), [arXiv:hep-ph/9710451](#); W. Beenakker, R. Hopker, M. Spira, and P. M. Zerwas, **B492**, 51 (1997), [arXiv:hep-ph/9610490](#).
- [67] V. Barger *et al.* (SUGRA Working Group Collaboration)(2000), [arXiv:hep-ph/0003154 \[hep-ph\]](#).
- [68] N. Bhattacharyya, A. Choudhury, and A. Datta, *Phys.Rev.* **D83**, 115025 (2011), [arXiv:1104.0333 \[hep-ph\]](#).
- [69] A. Djouadi, M. Muhlleitner, and M. Spira, *Acta Phys.Polon.* **B38**, 635 (2007), [arXiv:hep-ph/0609292 \[hep-ph\]](#).
- [70] M. Muhlleitner and E. Popenza, *JHEP* **1104**, 095 (2011), [arXiv:1102.5712 \[hep-ph\]](#).